Available online at www.sciencedirect.com
ScienceDirect
Carbohydrate Research 342 (2007) 1966–1973
Carbohydrate RESEARCH

Note

The conformational behaviour of the *C*-glycosyl analogue of sulfatide studied by NMR in SDS micelles

José Juan Hernández-Gay,[a] Luigi Panza,[b] Fiamma Ronchetti,[c] F. Javier Cañada,[a] Federica Compostella[c,*] and Jesús Jiménez-Barbero[a,*]

[a]*Departamento de Ciencia de Proteínas, Centro de Investigaciones Biológicas, CSIC, Ramiro de Maeztu 9, 28040 Madrid, Spain*
[b]*Dipartimento di Scienze Chimiche, Alimentari, Farmaceutiche e Farmacologiche, Università del Piemonte Orientale, Via Bovio 6, 28100-Novara, Italy*
[c]*Dipartimento di Chimica, Biochimica e Biotecnologie per la Medicina, Università di Milano, Via Saldini 50, 20133-Milano, Italy*

Received 9 March 2007; received in revised form 16 April 2007; accepted 22 April 2007
Available online 1 May 2007

Abstract—The conformational behaviour of sulfatide and its *C*-glycosyl analogue has been studied by using a combination of *J* and NOE data assisted by molecular mechanics calculations. There is a major exoanomeric conformation around the phi angle of both molecules with two or three conformers contributing to the equilibrium around psi. The MM3* calculations only provide a qualitative description of the actual population distribution. Despite this geometrical similarity, the quantitative analysis of the NOE intensities at a variety of mixing times indicates that the motion around the pseudoglycosidic linkages of the *C*-glycosyl analogue is faster than that for the natural compound.

Keywords: C-glycosides; Sulfatide; Micelles; NMR; Glycomimetics

Sulfatide is a mammalian sulfoglycolipid, which is a mixture of 3-*O*-sulfo-galactosylceramides containing fatty acid residues of different structure and chain length. The nervonoyl derivative is **1a**. Sulfatide is a major component of both the central and peripheral nervous systems, and is also present in subpopulations of neurons and astrocytes, which are nonmyelin-forming cells of the brain. This natural cellular lipid in myelin is localized to the plasma membrane, and functions as a structural component, while in neuron and astrocytes it is located in the intracellular compartment with functions not yet well understood.[1] It accumulates in these cells in arylsulfatase A (ASA)-deficient mice, which are a model for the human neurodegenerative disease metachromatic leukodystrophy.[2] Distinct sulfatide molecular species may have different distributions. For example, analysis in mice of the molecular species of sulfatide in cultured astrocytes and neurons showed that they contain mostly short-chain fatty acid sulfatide with an emphasis for stearic acid, while long-chain (C22–C26) fatty acids are found on sulfatide in myelin. The fatty acid chain length of sulfatide might determine its subcellular localization and thereby its function.[1] Furthermore, pancreatic islets are demonstrated to contain sulfatide and to exhibit a profile of species different from that of brain.[3]

Sulfatide is involved in immunological phenomena. In fact, in the context of the stimulation of T-cells mediated by CD1 proteins, sulfatide binds to all human CD1 molecules and also to mouse CD1d.[4] Treatment of wild-type (but not CD1d-deficient) mice with sulfatide prevented the development of experimental allergic encephalomyelitis (EAE).[5] Furthermore, antibodies to sulfatide occur in sera of some patients with demyelinating neuropathies and with newly diagnosed insulin-dependent diabetes mellitus caused by immunological destruction of insulin-secreting pancreatic islet β-cells.[6,7]

* Corresponding authors. E-mail addresses: federica.compostella@unimi.it; jjbarbero@cib.csic.es

0008-6215/$ - see front matter © 2007 Elsevier Ltd. All rights reserved.
doi:10.1016/j.carres.2007.04.023

Recently we have been involved in a study to evaluate how sulfatide structural modifications affect the T-cell response to this antigen mediated by CD1 proteins.[8,9] The importance of both the lipid and the sugar structure in the immunogenicity of these glycolipids is recognized. In particular, we prepared the *C*-glycosyl isosteric analogue of sulfatide to investigate whether the substitution of the anomeric oxygen with a methylene affects T-cell response.[10] Due to the well described conformational variations between *O*- and *C*-glycosyl compounds,[11] this modification might confer a different bound conformation[12] within the active site of CD1 molecules or might influence the binding capacity to CD1. Indeed, the biological results in the T-cell presentation assay have shown that C-sulfatide **1b** is less stimulatory than natural sulfatide **1a**.

Because the biological role of **1a** is related to a membrane-like environment, it is particularly important to study its conformation with amphiphilic molecules that might mimic the atmosphere of sulfatide incorporated into its biological environment, that is, with the lipid chains buried in a hydrophobic surrounding, better than in a nonpolar solvent or nonnatural medium, like DMSO or a water–hexane interface. Among these amphiphilic molecules, the most common membrane-mimicking aqueous media compatible with NMR studies in solution are detergents, such as sodium dodecyl sulfate (SDS). SDS can solubilize membrane lipopeptides or glycopeptides and form micelles of a few dozen molecules, which generally give a short enough correlation time for NMR studies in liquids. This led us to study the conformational behaviour of C-sulfatide **1b** in an SDS solution using NMR spectroscopy and to compare this with that of sulfatide **1a** itself.

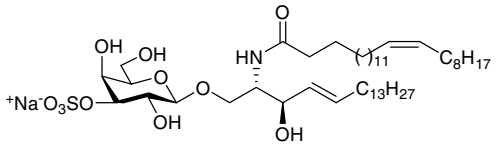

1a

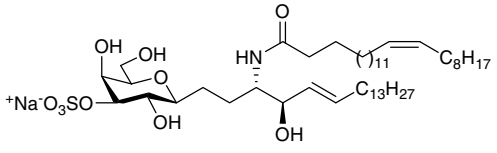

1b

Molecular mechanics and dynamics calculations: Molecular mechanics (MM) calculations were performed using the MM3* force field[13] as integrated in MACROMODEL.[14] The steric energy maps for **1a** and **1b** were computed as a function of the glycosidic (Φ) and aglyconic (Ψ) torsions, and the corresponding probability distributions were built from the relaxed maps, according to a Boltzmann function at 298 K (see figure in Supplementary data).

According to these calculations, the *O*-glycosyl compound presents three low-energy conformations, all of them showing the expected exoanomeric orientation around ϕ. Conformer A is located in the *exo*-ϕ/*anti*-ψ conformational region, conformer B shows *exo*-ϕ/*syn*-$\psi+$ geometry, while the global minimum C belongs to the *exo*-ϕ/*syn*-$\psi-$ area. The corresponding views of these conformers are given in Figure 1.

In contrast, for the *C*-glycosyl compound, the MM3* analysis predicts the presence of a rather distinct distribution. Again, three low-energy conformations are present, but in this case, not only the *exo*-ϕ configuration is populated, but also the global minimum is located in the *anti*-ϕ/*syn*-ψ region D. The *exo*-ϕ minima are located in the *exo*-ϕ/*anti*-ψA and *exo*-ϕ/*syn*-$\psi-$ C regions (Fig. 2).

The low-energy conformations obtained in the MM3* calculations were used as input structures for molecular dynamics (MD) simulations. These simulations were performed over 5 ns also using the same force field. The conformational behaviours of Φ and Ψ torsions were monitored during the simulation time and all the minima found in the MM calculations were shown to be conformationally stable (see figure in Supplementary data).

Indeed, for the *O*-glycosyl compound, the MD results are in good agreement with those predicted by MM, independent of the starting structure. The simulations predict that the glycosidic torsion only shows the *exo*-*syn* conformation, whereas for the aglyconic one, the three rotamers are present: *anti* (Ψ ca. 180°), $syn_{(-)}$ (Ψ ca. −90°) and $syn_{(+)}$ (Ψ ca. +120°). For **1b**, when the *exo*-Φ/*syn*-$\Psi-$ was used as input geometry, the simulation remained at this conformation for most of the time, with minor fluctuations to the *exo*-Φ/*anti*-Ψ geometry. The simulation starting at the global minimum *anti*-Φ/*syn*-Ψ conformer remained at this geometry for the whole trajectory.

NMR spectroscopy: The validity of the theoretical results was verified through NMR spectroscopy to assess the final conformational distribution for **1a** and **1b**. The chemical shifts in deuterated SDS micelles, in a 1:120 molar ratio, at 298 K are listed in Table 1, along with the scheme used for the atomic numbering. The assignment of the resonances was made using a combination of COSY, TOCSY, NOESY and HSQC experiments (see figure in Supplementary data).

The *J* values for the ring protons indicate that the pyranose rings adopt the usual $^4C_1$ chair conformation, independently of the nature of the C- or O-glycosidic linkage. The intermediate values observed for the C5–C6 lateral chains are in agreement with the well described equilibrium between the *tg*:*gt* conformers[15] for the Gal and pseudoGal rings of **1a** and **1b**, respectively.

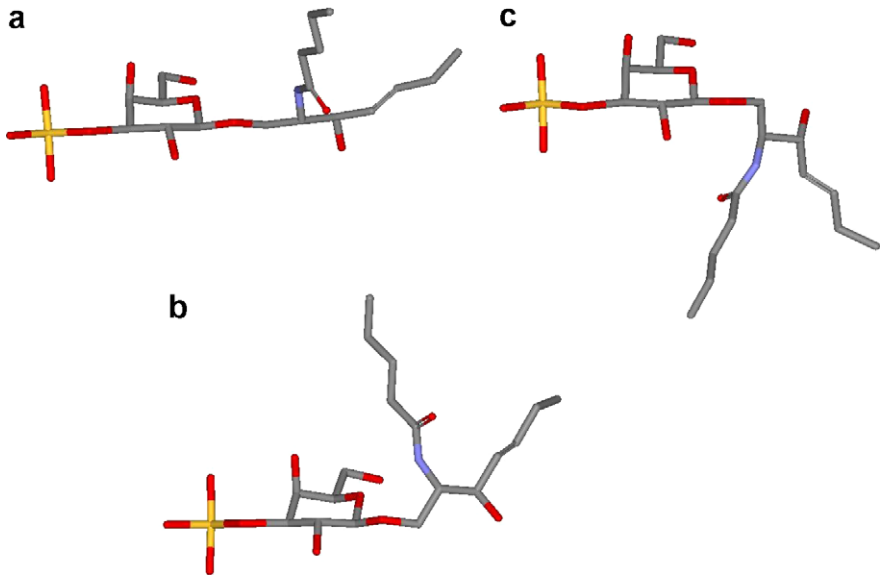

Figure 1. The most stable Φ, Ψ conformers of compound **1a**. (a) *exo*-Φ, *anti*-Ψ. (c) *exo*-Φ, *syn*-$\Psi_{(-)}$. (b) *exo*-Φ, *syn*-$\Psi_{(+)}$. A simplified model of the lipid tail has been used for simplicity.

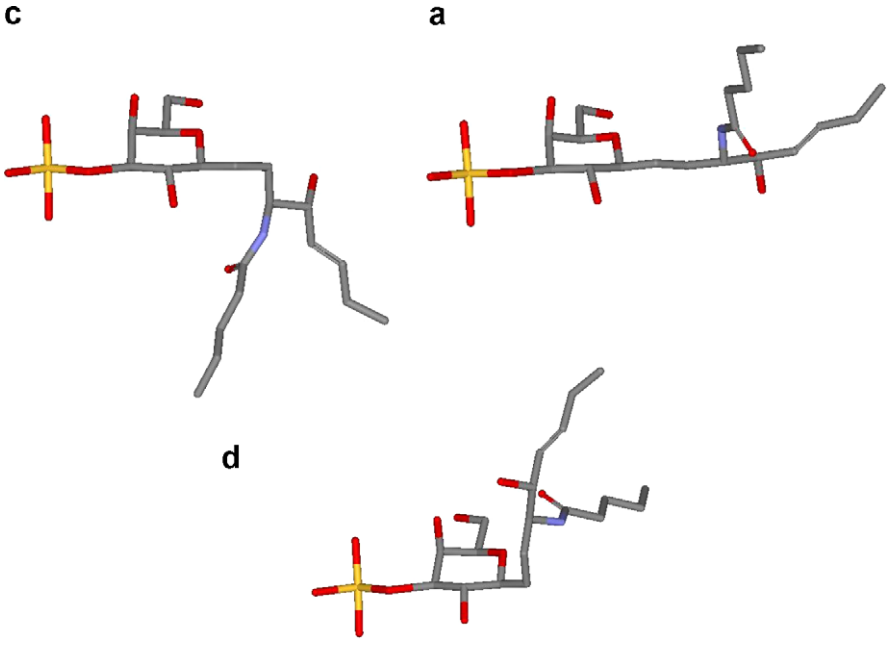

Figure 2. The most stable Φ, Ψ conformers of compound **1b**. (c) *exo*-Φ, *syn*-$\Psi_{(-)}$. (a) *exo*-Φ, *anti*-Ψ. (d) *anti*-Φ, *syn*-$\Psi_{(-)}$. A simplified model of the lipid tail has been used for simplicity.

For **1a**, no homonuclear couplings are available around the Φ glycosidic linkage, and thus the conformational distribution has to be derived from the NOE information,[16] assisted by the calculations.[17] In contrast, for **1b**, two interglycosidic couplings from Gal H1 (9.1, 2.1 Hz) could be measured. The existence of one large and one small value[18] is in agreement with the existence of a very major conformation around Φ, which corresponds to the *syn* exoanomeric orientation.[19] These coupling values allow us to discard the presence of the MM3*-based global minimum (*anti*-Φ) conformer in a significant amount. Thus, the MM3* calculations only provide a qualitative description of the actual population distribution, at least for compound **1b**.

Regarding Ψ angle, again, for **1a**, no homonuclear couplings are available,[18] and thus the assessment of the actual geometries has to rely on the combination of NOE data[16] and molecular mechanics.[17] For **1b**, although the $J_{CH2a,7a}$, $J_{CH2a,7b}$, $J_{CH2b,7a}$ and $J_{CH2b,7b}$ do indeed exist, they could not be measured in a reliable

Table 1. Chemical shifts (δ, ppm) and coupling constants (J, Hz) for the key protons of **1a** and **1b**[a]

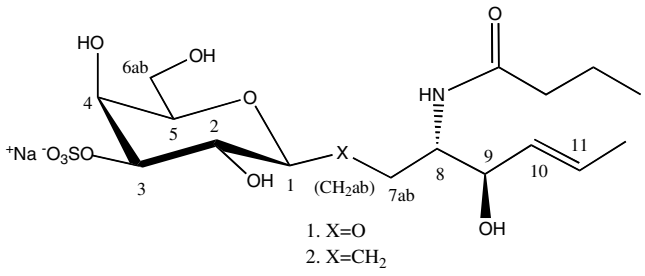

Compound **1a**	δ (ppm)	Compound **1b**	δ (ppm)
Gal H1	4.46	Gal H1	3.31
Gal H2	3.64	Gal H2	3.53
Gal H3	4.31	Gal H3	4.27
Gal H4	4.23	Gal H4	4.24
Gal H5	3.67	Gal H5	3.62
Gal H6a	3.78	Gal H6a	3.69
Gal H6b	3.78	Gal H6b	3.72
CH_{2a}	—	CH_{2a}	1.50
CH_{2b}	—	CH_{2b}	1.78
H_{7a}	4.01	H_{7a}	1.60
H_{7b}	3.87	H_{7b}	1.88
H_8	3.92	H_8	3.66
H_9	4.00	H_9	3.84
H_{10}	5.34	H_{10}	5.34
H_{11}	5.70	H_{11}	5.64
	(J, Hz)		(J, Hz)
$J_{1,2}$	8.0		9.3
$J_{2,3}$	10.1		9.3
$J_{3,4}$	4.3		3.5
$J_{4,5}$	<1		<1
$J_{5,6A}$	6.5		5.4
$J_{5,6B}$	7.6		8.0
$J_{7,8}$	8.5, 2.0		8.5, 2.0
$J_{8,9}$	9.0		8.5
$J_{9,10}$	9.0		8.5
$J_{10,11}$	15.0		15.2
$J_{11,12}$	6.8, 7.5		6.4, 7.4
$J_{1,CH2A}$	—		2.1
$J_{1,CH2B}$	—		9.1
$J_{7A,CH2A}$	—		Not measured
$J_{7A,CH2B}$	—		Not measured
$J_{7B,CH2A}$	—		Not measured
$J_{7B,CH2B}$	—		Not measured

[a] Measured at 1 mM concentration at 500 MHz in deuterated SDS micelles (120 mM) at 298 K.

manner and thus the protocol to obtain the distribution has to be as that used for **1a**.

There are three key additional torsional degrees of freedom that connect the lipid with the galactose/pseudogalactose moiety, dubbed as C7–C8, C8–C9 and C9–C10 linkages in the scheme given in Table 1. For both **1a** and **1b**, the corresponding coupling values could be measured and were found to be of similar values, within 0.5 Hz. This fact indicates that the conformational distribution around these three linkages is similar for both derivatives and, thus, the C-glycosidic linkage does not substantially influence the conformational behaviour of sulfatide at the lipid area. The $J_{8,9}$ and $J_{9,10}$ coupling values are equal or larger than 8.5 Hz, again indicating a major orientation around this area, with an *anti*-like relationship between both proton pairs. For the $J_{8,7a}$ and $J_{8,7b}$ couplings values of 2.1 and 9.1 Hz were found again, indicating the presence of a very major geometry around this linkage.

Then, the J-coupling information was complemented by the NOESY experiments (Table 2), which were carried out to finally deduce the conformational distributions for **1a** and **1b**. The intensities of the observed NOEs were transformed into distances, using a full matrix relaxation approach[16] and compared to those estimated by the molecular mechanics and dynamics calculations.[15,20] Indeed, the combination of NOESY/ROESY experiments showed that spin diffusion[15,16] is very efficient for both molecules, especially for **1b** (with the CH_2–CH_2– arrangement), under the employed experimental conditions and, thus, the use of a full relaxation matrix approach is a must.

The key NOEs for the conformational information around Φ, Ψ are those involving Gal H1 and the proximal protons of the lipid moiety. In all cases, NOEs were negative; that is, they showed the same sign as the diagonal peaks.[16] For **1a**, these key NOEs were transformed into distances using a full relaxation matrix approach as described, and compared to those obtained from the low-energy structures calculated by MM3*. From this comparison, it can be deduced that no single conformer may exclusively explain the observed NOEs. Indeed, according to the NOE data, **1a** exists as a conformational equilibrium among the three predicted conformers. The best fit between observed and predicted NOE data (Table 3) was obtained when there was a population distribution of approximately 40% of the *exo*-ϕ/*anti*-ψ conformer, 10% of the *exo*-ϕ/*syn*-$\psi(-)$ conformer and 50% of the *exo*-ϕ/*syn*-ψ conformer. A view of these

Table 2. Selected NOEs at 200 ms mixing time for the anomeric proton (H1 Gal) of **1a** and **1b**[a]

	Observed NOE % (200 ms mixing time)
Compound **1a**	
Gal H1/Gal H3	11
Gal H1/CH_2b	5
Gal H1/H8	3
Gal H1/CH_2a	8
Gal H1/Gal H2+H5	10
Compound **1b**	
Gal H1/CH_2-b	2
Gal H1/CH_2-a	4
Gal H1/H_7a	2
Gal H1/H_7b	4
Gal H1/H8	4
Gal H1/Gal H2	3
Gal H1/Gal H3+H4	13

[a] Measured at 1 mM concentration at 500 MHz in deuterated SDS micelles (120 mM) at 298 K.

Table 3a. Experimental inter-proton distances from NOE analysis according to a full relaxation matrix approach, for the anomeric proton H1 Gal of **1a**[a]

Proton pair	Exp. distance (Å)	Φ 50/ψ 180 (Å)	Φ 60/ψ −60 (Å)	Φ 60/ψ 120 (Å)	Average $\langle r^{-6}\rangle^{-1/6}$ 40/10/50 A/B/C distribution (Å)
H1/H_7a	2.8	2.4	3.0	3.2	2.7
H1/H8	3.2	4.2	2.2	4.6	3.2
H1/H_7b	2.6	2.9	3.7	2.3	2.5

[a] Measured at 1 mM concentration at 500 MHz in deuterated SDS micelles (120 mM) at 298 K.

Table 3b. Fitting of the observed NOEs to the experimental values for the different proton pairs regions of **1b**[a,b]

	τ_c 1500 ps		Exp
	Φ70 Ψ −55	Φ60 Ψ −175	
Gal H1/Gal H3+H4	11+2%	10%+2%	13%
Gal H1/Gal H2	4%	4%	3%
	τ_c 800 ps		
Gal H1/CH_2b	2%	2%	2%
Gal H1/CH_2a	4%	4%	4%
Gal H1/H_7a	1%	2%	2%
Gal H1/H_7b	1%	4%	4%
Gal H1/CHNH	6%	0%	3%

[a] Measured at 500 MHz, 298 K with 200 ms mixing time.
[b] The required effective correlation time for fitting the intra-residue cross peaks within the six-membered ring is different to that required for the inter-residue ones.

conformers is given in Figure 1 and its superimposition in Figure 3. In any case, the long lipid tails may adopt a variety of orientations in the SDS medium, as also depicted in Figure 3.

For compound **1b**, again, the calculations are compared with the experimental data, to conclude that this compound populates the *exo*-ϕ/*anti*-ψ and *exo*-ϕ/*syn*-$\psi_{(-)}$ minima. Nevertheless, by using a single global motion rotational correlation time, it was also impossible to quantitatively fit, in a simultaneous manner, all the cross peaks belonging to the different parts of the molecule (Table 3). Thus, different effective correlation times were used for the intra-sugar cross peaks for the sugar–lipid cross peaks, and for the intra-lipid cross peaks. This is a clear indication of internal flexibility of this molecule, with distinct motion in the different parts of the molecule. Indeed, when the NOEs of the sugar ring were adjusted, using 1500 ps as correlation time, the sugar–lipid and the lipid NOEs were overestimated. In contrast, when the correlation time was decreased to 800 ps, indicating a faster motion around this area, it was possible to adjust the experimental with the simulated sugar–lipid NOEs, assuming a conformational equilibrium, in which the *exo*-ϕ/*anti*-ψ and *exo*-ϕ/*syn*-$\psi_{(-)}$ geometries are equally present in approximately 50%.

The coupling values for the H7/H8, H8/H9 and H9/H10 proton pairs (see Table 1), as well as the observed NOEs within the C7–C11 fragment, are in agreement with a major *anti*, *anti* orientation for the O(CH_2)–C7–C8–C9, C7–C8–C9–C10 linkages and a value around −140° for the C8–C9–C10–C11 torsion for both **1a** and **1b**.

In conclusion, the conformational behaviour for sulfatide and its *C*-glycosyl analogue is relatively similar in terms of the contributing conformations. According to the combination of *J* and NOE with the geometries provided by molecular mechanics calculations,[15] there is a major exoanomeric conformation around the Φ angle of both molecules with two or three conformers contributing to the equilibrium around Ψ. Nevertheless, the MM3* calculations only provide a qualitative description of the actual population distribution. The existence of a major exoanomeric orientation for the *C*-glycosyl compound is due to the steric interaction between the equatorial O-2 and the aglycon in the non-exoanomeric orientation.[21] Despite this geometrical similarity, the quantitative analysis of the NOE intensities at a variety of mixing times indicates that the motion around the pseudoglycosidic linkages of the *C*-glycosyl analogue **1b** is faster than that for **1a**. The importance of this feature for the observed decreased stimulatory activity of **1b** versus **1a** remains an open question and has to be further evaluated. At this point we propose, although merely speculatively, that the reduced potency of **1b** versus **1a** might be related to their different conformational distributions, the different dynamic behaviour or simply to the requirement of the glycosidic oxygen to establish key interactions with its environment. Nevertheless, although relatively large doses of C-sulfatide **1b** are required to generate a sufficient number of stimulatory CD1a complexes, the enhanced stability of this molecule towards chemical and biological degradation makes it a good candidate for further research in this area.

1. Experimental

1.1. Materials

Compounds **1a** and **1b** were obtained as previously described.[8,10]

1.2. Molecular mechanics calculations

The relaxed (ϕ,ψ) energy maps for compounds **1a** and **1b** were generated by systematic rotations around the

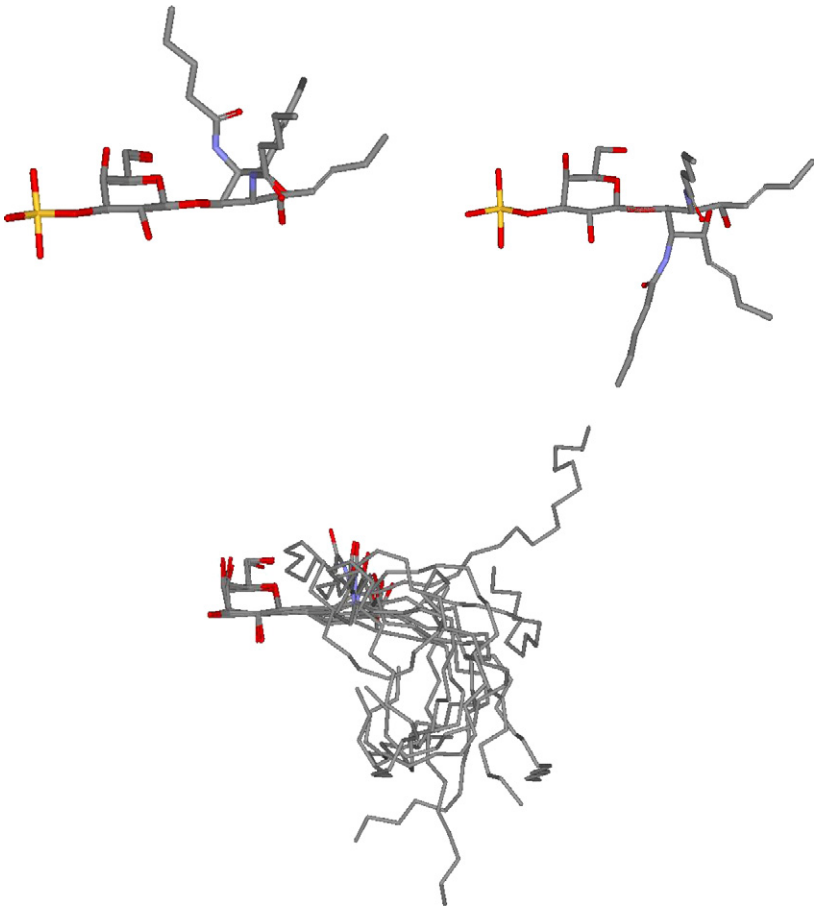

Figure 3. Superimposition of the two major Φ, Ψ conformers for compounds **1a** (left) and **1b** (right). For **1a**, they are the *exo*-Φ, *anti*-Ψ and the *exo*-Φ, *syn*-$\Psi_{(+)}$. For **1b**, the *exo*-Φ, *anti*-Ψ and the *exo*-Φ, *syn*-$\Psi_{(-)}$. A simplified model of the lipid tail has been used for simplicity. A superimposition of six conformers randomly taken from snapshots of the MD simulation is shown below, to show the large conformational space encompassed by the lipid tails. In this case, the sulfate group has been removed from the superimposition.

glycoside and aglyconic bond using a grid step of 18°, optimization of the geometry at every Φ, Ψ point using conjugate gradients iterations until the rms derivative was smaller than 0.05 kJ mol^{-1} Å^{-1}, and energy calculation using the MM3* force field ($\varepsilon = 80$) as integrated in MAESTRO program. The *tg* and *gt* orientations of the lateral chain of the galactose moiety[22] were taken into account, because they have been shown to be much more stable than the alternative *gg* conformer. Thus, two starting structures were considered, and in total, 800 conformers calculated. From these relaxed energy maps, adiabatic surfaces were built by choosing the lowest energy structure for a given ϕ, ψ point. The probability distribution was calculated for each point according to a Boltzmann function at 298 K.

1.3. *J* and NOE calculations

The vicinal coupling constants were calculated for each conformation using the Karplus–Altona equation.[18] Ensemble average values were calculated from the distribution according to $J = \sum P_{\phi\psi} J_{i\phi\psi}$. The interproton average distances were calculated using the following expression: $\langle r^{-6} \rangle_{kl} = \sum P_{\phi\psi} r^{-6}_{kl(\phi\psi)}$. To deduce the interproton distances, relaxation matrix calculations were performed using the software written in our laboratories that is available from the authors upon request.[23] Isotropic motion and external relaxation of 0.1 s^{-1} was first assumed. Nevertheless, by using a single global motion rotational correlation time, it was also impossible to quantitatively fit, in a simultaneous manner, all the cross peaks belonging to the different parts of the molecule. Thus, different effective correlation times were used for the intra-sugar cross peaks, for the sugar–lipid cross peaks, and for the intra-lipid cross peaks. This is a clear indication of internal flexibility of this molecule with distinct motion in the different parts of the molecule.[24] Within the sugar ring, a correlation time of 1500 ps was used to obtain the best matching between experimental and calculated NOEs for the intraresidue H1–H3 proton pair.

1.4. NMR spectroscopy

Each molecule (ca. 1 mM) was dissolved in aqueous (D_2O), micellar solutions of 120 mM SDS-d_{25} (Eurisotop), and the pH was adjusted to 5.1. NMR experiments were recorded on a Bruker Avance 500 instrument at 25 °C. Chemical shifts were referenced to external DSS in D_2O. 1D spectra were acquired using 32K data points, which were zero-filled to 64 K data points prior to Fourier transformation. Absolute value COSY, and phase-sensitive HSQC spectra, NOESY and ROESY (mixing times of 200, 300 and 400 ms) were acquired using standard techniques. Acquisition data matrices were defined by $2K \times 256$ points, multiplied by appropriate window functions and zero-filled to $2K \times 512$ matrices prior to Fourier transformation. Baseline correction was applied in both dimensions. 1D-selective NOE spectra were acquired using the double echo sequence proposed by Shaka and co-workers[25] at four different mixing times (200–600 ms). Spectra were processed using the Bruker XWIN-NMR program on a personal computer.

Acknowledgements

Financial support by the Ministry of Education and Science of Spain (CTQ-2006-10874-C02-01) and by MIUR-Italy (FIRB 2001) is gratefully acknowledged, as is a EC Marie Curie Research Training Network grant (Contract No: MRTN-CT-2005-019561). The CAI-NMR facility at the University Complutense of Madrid is thanked for the access to the 500 MHz spectrometer.

Supplementary data

Supplementary data associated with this article can be found, in the online version, at doi:10.1016/j.carres.2007.04.023.

References

1. Isaac, G.; Pernber, Z.; Gieselmann, V.; Hansson, E.; Bergquist, J.; Månsson, J.-E. *FEBS J.* **2006**, *273*, 1782–1790, and references cited therein.
2. Molander-Melin, M.; Pernber, Z.; Franken, S.; Gieselmann, V.; Mansson, J. E.; Fredman, P. *J. Neurocytol.* **2004**, *33*, 417–427.
3. Hsu, F. F.; Bohrer, A.; Turk, J. *Biochim. Biophys. Acta* **1998**, *1392*, 202–216.
4. De Libero, G.; Mori, L. *Nat. Rev. Immunol.* **2005**, *5*, 485–496.
5. Jahng, A.; Maricic, I.; Aguilera, C.; Cardell, S.; Halder, R. C.; Kumar, V. *J. Exp. Med.* **2004**, *199*, 947–957.
6. Fredman, P.; Lycke, J.; Andersen, O.; Vretham, M.; Ernerudh, J.; Svennerholm, L. *J. Neurol.* **1993**, *240*, 381–387.
7. Buschard, K.; Josefsen, K.; Horn, T.; Fredman, P. *Lancet* **1993**, *342*, 840.
8. Compostella, F.; Franchini, L.; De Libero, G.; Palmisano, G.; Ronchetti, F.; Panza, L. *Tetrahedron* **2002**, *58*, 8703–8708.
9. Compostella, F.; Ronchi, S.; Panza, L.; Mariotti, S.; Mori, L.; De Libero, G.; Ronchetti, F. *Chem. Eur. J.* **2006**, *12*, 5587–5595.
10. Modica, E.; Compostella, F.; Colombo, D.; Franchini, L.; Cavallari, M.; Mori, L.; De Libero, G.; Panza, L.; Ronchetti, F. *Org. Lett.* **2006**, *8*, 3255–3258.
11. (a) Jiménez-Barbero, J.; Espinosa, J. F.; Asensio, J. L.; Cañada, F. J.; Poveda, A. The conformation of *C*-glycosyl compounds. In *Adv. Carbohydr. Chem. Biochem.*; Horton, D., Ed.; Academic Press, 2001; Vol. 56, pp 235–284; (b) Espinosa, J. F.; Bruix, M.; Jarreton, O.; Skrydstrup, T.; Beau, J.-M.; Jiménez-Barbero, J. *Chem. Eur. J.* **1999**, *5*, 442–448; (c) Espinosa, J. F.; Martín-Pastor, M.; Asensio, J. L.; Dietrich, H.; Martín-Lomas, M.; Schmidt, R. R.; Jiménez-Barbero, J. *Tetrahedron Lett.* **1995**, *36*, 6329–6332; (d) Vidal, P.; Vauzeilles, B.; Blériot, Y., Sollogoub, M.; Sinaÿ, P.; Espinosa, J. F.; Jiménez-Barbero, J. *Carbohydr. Res.*, this issue, doi:10.1016/j.carres.2007.04.017.
12. (a) Espinosa, J.-F.; Cañada, F. J.; Asensio, J. L.; Martín-Pastor, M.; Dietrich, H.; Martín-Lomas, M.; Schmidt, R. R.; Jiménez-Barbero, J. *J. Am. Chem. Soc.* **1996**, *118*, 10862–10871; (b) Carpintero, M.; Bastida, A.; Garcia-Junceda, E.; Jimenez-Barbero, J.; Fernandez-Mayoralas, A. *Eur. J. Org. Chem.* **2001**, 4127–4135; (c) Asensio, J. L.; Espinosa, J. F.; Dietrich, H.; Cañada, F. J.; Schmidt, R. R.; Martín-Lomas, M.; André, S.; Gabius, H.-J.; Jiménez-Barbero, J. *J. Am. Chem. Soc.* **1999**, *121*, 8995–9000; (d) García-Aparicio, V.; Sollogoub, M.; Blériot, Y.; Colliou, V.; André, S.; Asensio, J. L.; Cañada, F. J.; Gabius, H.-J.; Sinaÿ, P.; Jiménez-Barbero, J. *J. Carbohydr. Res.*, this issue, doi:10.1016/j.carres.2007.02.034.
13. Allinger, N. L.; Yuh, Y. H.; Lii, J. H. *J. Am. Chem. Soc.* **1989**, *111*, 8551–8566.
14. Mohamadi, F.; Richards, N. G. J.; Guida, W. C.; Liskamp, R.; Lipton, M.; Caufield, C.; Chang, G.; Hendrickson, T.; Still, W. C. J. *Comp. Chem.* **1990**, *11*, 440–467.
15. For a survey of NMR methods and data applied to saccharide molecules, see: *NMR Spectroscopy of Glycoconjugates*; Jiménez-Barbero, J., Peters, T., Eds.; Weinheim: Wiley-VCH, 2002.
16. Neuhaus, D.; Williamson, M. P. *The Nuclear Overhauser Effect in Structural and Conformational Analysis*; VCH: New York, 1989.
17. For the application of molecular mechanics force fields to the conformational analysis of carbohydrate molecules, see: Perez, S.; Imberty, A.; Engelsen, S.; Gruza, J.; Mazeau, K.; Jimenez-Barbero, J.; Poveda, A.; Espinosa, J. F.; van Eyck, B. P.; Johnson, G.; French, A. D.; Kouwijzer, M. L. C. E.; Grootenuis, P. D. J.; Bernardi, A.; Raimondi, L.; Senderowitz, H.; Durier, V.; Vergoten, G.; Rasmussen, K. *Carbohydr. Res.* **1998**, *314*, 141–155.
18. Haasnoot, C. A. G.; de Leeuw, F. A. A. M.; Altona, C. *Tetrahedron* **1980**, *36*, 2783–2792.
19. See: *The Anomeric Effect: Origin and Consequences*; Szarek, W. A., Horton, D., Eds. American Chem. Soc. Symp. Ser. 87; ACS: Washington, DC, 1979.
20. For instance, see: Martin-Pastor, M.; Espinosa, J. F.; Asensio, J. L.; Jimenez-Barbero, J. *Carbohydr. Res.* **1997**, *298*, 15–49.

21. Asensio, J. L.; Cañada, F. J.; Garcia-Herrero, A.; Murillo, M. T.; Fernández-Mayoralas, A.; Johns, B. A.; Kozak, J.; Zhu, Z. Z.; Johnson, C. R.; Jiménez-Barbero, J. *J. Am. Chem. Soc.* **1999**, *121*, 11318–11329.
22. See for instance: *Computer Modelling of Carbohydrate Molecules* French, A. D., Brady, J. W., Eds.; Am. Chem. Soc. Symp. Ser.; Washington, DC, 1990.
23. For instance: Asensio, J. L.; Cañada, F. J.; Kahn, N.; Mootoo, D. A.; Jiménez-Barbero, J. *Chem. Eur. J.* **2000**, *6*, 1035–1041.
24. Poveda, A.; Asensio, J. L.; Martín-Pastor, M.; Jimenez-Barbero, J. *J. Biomol. NMR* **1997**, *10*, 29–43.
25. Stott, K.; Stonehouse, J.; Keeler, J.; Hwang, T.-L.; Shaka, A. J. *J. Am. Chem. Soc.* **1995**, *117*, 4199–4200.